

Electronic structure of a narrow-gap semiconductor KAg_3Te_2

Rong Feng(冯荣), Haotian Zheng(郑昊天), Haoran Liu(刘浩然), Binru Zhao(赵彬茹), Xunqing Yin(尹训庆), Zhihua Liu(刘智华), Feng Liu(刘峰), Guohua Wang(王国华), Xiaofeng Xu(许晓峰), Wentao Zhang(张文涛), Weidong Luo(罗卫东), Wei Zhou(周苇), and Dong Qian(钱冬)

Citation: Chin. Phys. B, 2025, 34 (**4**): 047102. DOI: 10.1088/1674-1056/adb680
Journal homepage: http://cpb.iphy.ac.cn; http://iopscience.iop.org/cpb

What follows is a list of articles you may be interested in

Visualizing the electronic structure of kagome magnet $LuMn_6Sn_6$ by angle-resolved photoemission spectroscopy

Man Li(李满), Qi Wang(王琦), Liqin Zhou(周丽琴), Wenhua Song(宋文华), Huan Ma(马欢), Pengfei Ding(丁鹏飞), Alexander Fedorov, Yaobo Huang(黄耀波), Bernd Büchner, Hechang Lei(雷和畅), Shancai Wang(王善才), and Rui Lou(娄睿)

Chin. Phys. B, 2024, 33 (**11**): 117101. DOI: 10.1088/1674-1056/ad7afe

Coexistence of Dirac and Weyl points in non-centrosymmetric semimetal $NbIrTe_4$

Qingxin Liu(刘清馨), Yang Fu(付阳), Pengfei Ding(丁鹏飞), Huan Ma(马欢), Pengjie Guo(郭朋杰), Hechang Lei(雷和畅), and Shancai Wang(王善才)

Chin. Phys. B, 2024, 33 (**4**): 047104. DOI: 10.1088/1674-1056/ad2a79

Angle-resolved photoemission study of NbGeSb with non-symmorphic symmetry

Huan Ma(马欢), Ning Tan(谭宁), Xuchuan Wu(吴徐传), Man Li(李满), Yiyan Wang(王义炎), Hongyan Lu(路洪艳), Tianlong Xia(夏天龙), and Shancai Wang(王善才)

Chin. Phys. B, 2024, 33 (**2**): 027102. DOI: 10.1088/1674-1056/ad0ccf

Electronic structure study of the charge-density-wave Kondo lattice $CeTe_3$

Bo Wang(王博), Rui Zhou(周锐), Xuebing Luo(罗学兵), Yun Zhang(张云), and Qiuyun Chen(陈秋云)

Chin. Phys. B, 2023, 32 (**9**): 097103. DOI: 10.1088/1674-1056/acb41e

Single crystal growth and electronic structure of Rh-doped $Sr_3Ir_2O_7$

Bingqian Wang(王冰倩), Shuting Peng(彭舒婷), Zhipeng Ou(欧志鹏), Yuchen Wang(王宇晨), Muhammad Waqas, Yang Luo(罗洋), Zhiyuan Wei(魏志远), Linwei Huai(淮琳崴), Jianchang Shen(沈建昌), Yu Miao(缪宇), Xiupeng Sun(孙秀鹏), Yuewei Yin(殷月伟), and Junfeng He(何俊峰)

Chin. Phys. B, 2023, 32 (**8**): 087108. DOI: 10.1088/1674-1056/acd7d5

Electronic structure of a narrow-gap semiconductor KAg_3Te_2

Rong Feng(冯荣)[1], Haotian Zheng(郑昊天)[1], Haoran Liu(刘浩然)[1], Binru Zhao(赵彬茹)[1], Xunqing Yin(尹训庆)[1], Zhihua Liu(刘智华)[1], Feng Liu(刘峰)[1], Guohua Wang(王国华)[1], Xiaofeng Xu(许晓峰)[2], Wentao Zhang(张文涛)[1,3], Weidong Luo(罗卫东)[1], Wei Zhou(周苇)[4], and Dong Qian(钱冬)[1,5,6,†]

[1] *Key Laboratory of Artificial Structures and Quantum Control (Ministry of Education), School of Physics and Astronomy, Shanghai Jiao Tong University, Shanghai* 200240, *China*

[2] *School of Physics, Zhejiang University of Technology, Hangzhou* 310023, *China*

[3] *Institute of Physics, Chinese Academy of Sciences, Beijing* 100190, *China*

[4] *School of Electronic and Information Engineering, Changshu Institute of Technology, Changshu* 215500, *China*

[5] *Collaborative Innovation Center of Advanced Microstructures, Nanjing University, Nanjing* 210093, *China*

[6] *Tsung-Dao Lee Institute, Shanghai Jiao Tong University, Shanghai* 200240, *China*

(Received 2 January 2025; revised manuscript received 13 February 2025; accepted manuscript online 15 February 2025)

KAg_3Te_2 with a layered crystal structure has been predicted to be a possible topological insulator. Through electrical transport measurements, we revealed its semiconducting behavior with a narrow band gap of ~ 0.4 eV and p-type character. The infrared transmission spectra of single crystals yielded an optical band gap of ~ 0.3 eV. Angle-resolved photoemission spectroscopy reveals a bulk energy gap at the Brillouin zone center, with no observable surface state, suggesting that KAg_3Te_2 is a topological trivial narrow-gap semiconductor. The experimentally determined effective mass of the holes in KAg_3Te_2 is very small ($\sim 0.12\ m_e$). The valence band maximum is quasi-two-dimensional, while the conduction band minimum is fully three-dimensional. Such intriguing dimensional anisotropy can be attributed to the distinct orbital contributions from K, Ag, and Te atoms to the respective bands.

Keywords: KAg_3Te_2 crystals, narrow-gap semiconductor, angle-resolved photoemission spectroscopy, small effective hole mass, dimensional anisotropy

PACS: 71.20.Nr, 79.60.–i, 71.20.–b

DOI: 10.1088/1674-1056/adb680 **CSTR:** 32038.14.CPB.adb680

1. Introduction

Many excellent thermoelectric (TE) materials are also known as topological insulators (TIs),[1–5] as TE and TI compounds often share similar material features, such as the present of heavy elements and narrow bulk band gaps. Narrow gap $CsAg_3S_2$-type[6] isostructures, such as KAg_3Te_2, KAg_3Se_2, and $RbAg_3Se_2$, have attracted much attention due to their promising thermoelectric properties.[7–10] These materials are classified differently in two database: one classified them as TIs,[11] while the other categorizes them as topological trivial narrow-gap semiconductors.[12] The inconsistency in the identification of topological property requires the direct measurements of the electronic structures of $CsAg_3S_2$-type materials.

In this work, we studied the electronic structure of KAg_3Te_2 single crystals through electrical transport, optical absorption, angle-resolved photoemission spectroscopy (ARPES) and first-principles calculations. Our findings reveal that KAg_3Te_2 is a narrow-gap semiconductor with a highly dispersive valence band around Brillouin zone center. The hole's effective mass is about 0.12 m_e. The experimental determined bulk energy gap is approximately 0.3 eV–0.4 eV. No surface state was observed, which indicates that KAg_3Te_2 is a topological trivial narrow-gap semiconductor. Near the Fermi energy, the highest valence band exhibits quasi-two-dimensional characteristics, while the lowest conduction band shows fully three-dimensional behavior. The small hole mass and the pronounced dimensional anisotropy between the valence and conduction bands may have potential applications in the future.

2. Methods

KAg_3Te_2 single crystals were synthesized by reacting a stoichiometric mixture of K (99%), Ag-grain (99.99%), and Te-powder (99.999%) in an evacuated quartz tube. The mixture was heated to 1223 K for 36 hours, melted completely, and then slowly cooled to ambient temperature at a rate of 2 K/h. The x-ray diffraction (XRD) using Cu K_α radiation and x-ray Laue diffraction verified the crystal structure and orientation of the crystals.

The electric transport properties were measured using the physical property measurement system (PPMS). Infrared transmission spectra were obtained at room temperature using a Fourier transform infrared spectrometer in conjunction with

†Corresponding author. E-mail: dqian@sjtu.edu.cn

© 2025 Chinese Physical Society and IOP Publishing Ltd. All rights, including for text and data mining, AI training, and similar technologies, are reserved.

an infrared microscope. The spot size is about 10 μm×10 μm. Laser-based ARPES measurements were carried out with a 6.05 eV laser. Synchrotron-based ARPES measurements were performed at beamline 03U of the Shanghai Synchrotron Radiation Facility. Scienta DA30-L-8000R electron analyzer was used. Angular resolution is ∼ 0.1° and energy resolution is ∼ 15 meV. Samples were cleaved *in situ* in the ultra-high vacuum chamber and ARPES spectra were collected above 125 K to avoid charging effect at lower temperatures.

First-principles calculations were carried out with the Vienna *ab initio* simulation package (VASP).[13,14] All calculations were performed with the generalized gradient approximation of the Perdew–Burke–Ernzerhof (GGA-PBE) formula.[15] The electronic wave function is expended using the plane-wave basis with a kinetic-energy cutoff of 500 eV. The k-point sampling in the first Brillouin zone (BZ) is done over an 8×8×4 Γ-centered Monkhorst–Pack k-mesh.[16] For structural optimization, the atomic positions are relaxed until the force on each atom is less than 0.005 eV/Å.

3. Results and discussion

3.1. Crystal structure

KAg_3Te_2 crystallizes in a monoclinic structure with space group $C2/m$ (No. 12), isotypic with $CsAg_3S_2$.[6] As shown in Figs. 1(a) and 1(b), KAg_3Te_2 has a layered structure. The $[Ag_3Te_2]^-$ layer mainly involves distorted tetrahedra $AgTe_4$. Alternating layers of K^+ cations and $[Ag_3Te_2]^-$ anions stack along c-axis suggests that the natural cleavage surface will be (001) plane. Inset of Fig. 1(b) shows an optical image of a crystal. The shining surface is (001) plane. XRD spectrum of KAg_3Te_2 crystals shows sharp (00l) peaks (Fig. 1(b)). The sharp Laue pattern from the cleaved plane indicates good crystallinity of the sample.

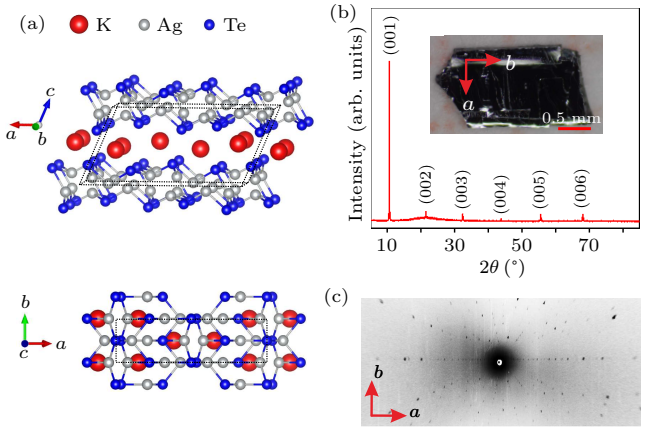


Fig. 1. Crystal structure of KAg_3Te_2. (a) Schematic lattice structure of KAg_3Te_2. Dotted lines indicate the conventional unit cell. (b) XRD spectrum with sharp (00l) diffraction peaks. The inset is an optical image of a freshly cleaved crystal. (c) Laue back reflection pattern from the (001) plane.

3.2. Electrical transport and infrared absorption

The resistivity of KAg_3Te_2 as a function of temperature, measured by the standard four-probe method, is shown in Fig. 2(a), which exhibits insulating behavior. An Arrhenius plot fitting $\left(R = A\exp\left(\frac{\Delta}{2k_BT}\right)\right)$ yields a band gap of about 0.4 ± 0.1 eV. The inset of Fig. 2(a) shows that the Hall voltage lineally depends on the applied magnetic field at 300 K. According to the resistivity and Hall measurement, our KAg_3Te_2 crystal is a p-type semiconductor with a hole concentration of about 6.1×10^{14} cm^{-3} and a Hall mobility of ~ 38 cm$^2\cdot$V$^{-1}\cdot$s^{-1} at 300 K.

The band gap is also extracted from the infrared transmission spectra. We considered KAg_3Te_2 as a direct-gap semiconductor and plotted $(\alpha h\nu)^2$ as a function of $h\nu$, called Tauc plot in Fig. 2(b), where α is the absorption coefficient and $h\nu$ is the photon energy. The three small peaks below 0.3 eV likely originated from ambient atmospheric interferences. Fitting a straight line to the linear region (Tauc line, red dashed line in Fig. 2(b)) to intersect the linear fitting baseline (blue dashed line in Fig. 2(b)) yields an optical band gap of ∼ 0.3 eV. The optical band gap is compatible with the gap obtained from the resistivity measurements.

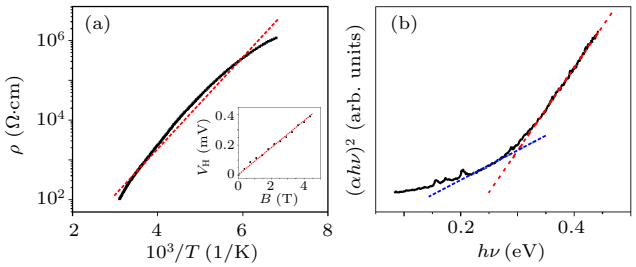


Fig. 2. (a) Temperature-dependent resistivity of KAg_3Te_2 from 147 K to 322 K. Red dashed line is the Arrhenius plot fitting. Inset is the Hall voltage as a function of magnetic field at 300 K. Red dashed line is a linear fitting. (b) Tauc plot of absorption curve assuming a direct energy gap.

3.3. ARPES measurements and first-principles calculations

Figure 3(a) shows the bulk BZ and its surface projection onto the (001) surface. Figure 3(b) presents a constant energy mapping at binding energy of −0.2 eV in the $\bar{C}$–$\bar{\Gamma}$–$\bar{Y}$ plane using incident photons of $h\nu = 70$ eV. Green dashed lines indicate the surface BZ. Apart from some spectral intensity around the $\bar{\Gamma}$ point, there is no other distinct feature within the surface BZ. Figures 3(c) and 3(d) show the ARPES spectra (left) and corresponding secondary derivative image plots (right) along $\bar{C}$–$\bar{\Gamma}$–$\bar{C}$ and $\bar{Y}$–$\bar{\Gamma}$–$\bar{Y}$ directions in the second surface BZ (indicated by cut-1 and cut-2 in Fig. 3(b)). Clearly, there are several hole-like bands below the Fermi energy, with the band maximum locates at $\bar{\Gamma}$ point. Figure 3(e) depicts four ARPES spectra near the Fermi energy along $\bar{C}$–$\bar{\Gamma}$–$\bar{C}$ direction, using incident photon energies of 6.05 eV, 62 eV, 70 eV, and 78 eV. The band maximum of the highest valence band is at about 0.2 eV below Fermi level and remains nearly unchanged within the

experimental uncertainty for different incident photon energies. No metallic surface bands were observed, which suggests that KAg_3Te_2 is topological trivial. Other valence bands shift upwards when using incident photons of 62 eV, 70 eV or 78 eV. Changing the incident photon energy in ARPES experiments corresponds to change in k_z. Thus, the highest valence band appears to have little dispersion along k_z direction compared to other valence bands. The parabola fitting of the highest valence band yields a very small effective hole mass of about 0.12 m_e. We compared the energy gap and hole mass of KAg_3Te_2 with several narrow-gap semiconductors in Table 1. The data were primarily obtained near room temperature (RT), unless otherwise specified in the table.

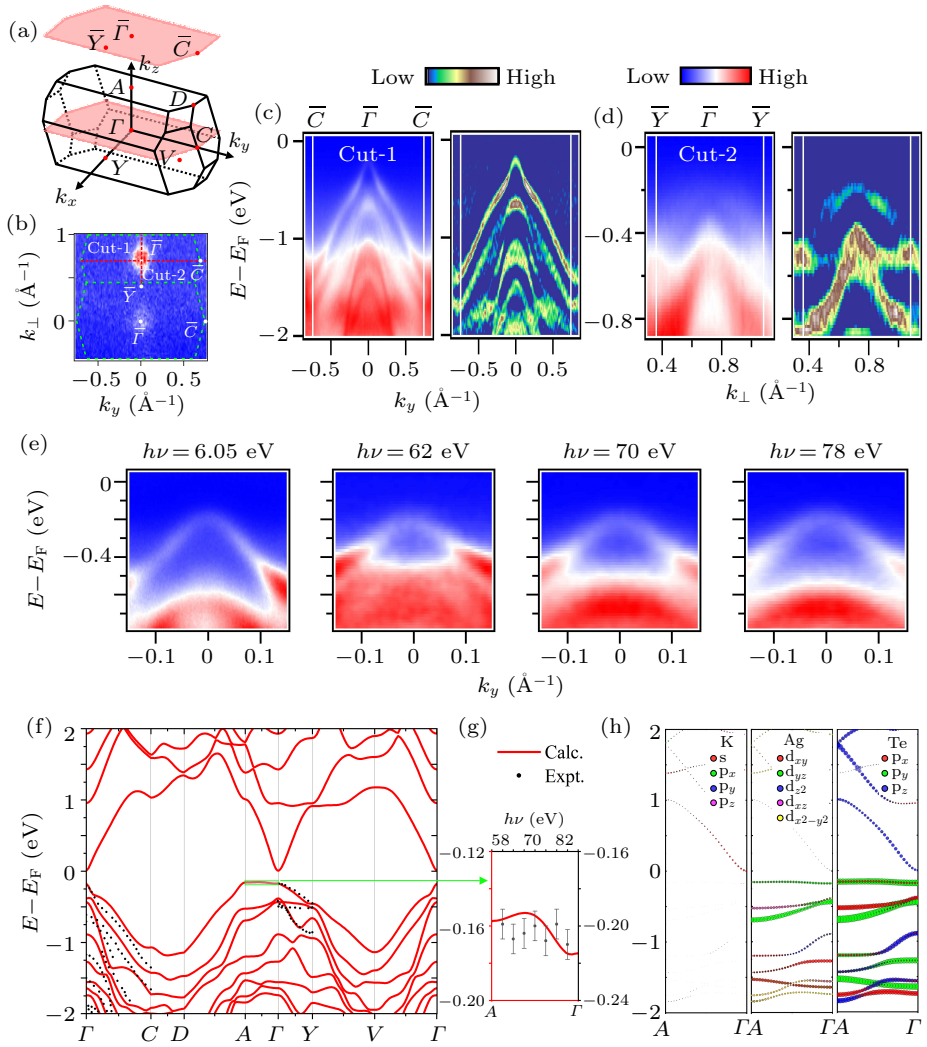


Fig. 3. (a) The bulk BZ and the projected BZ of (001) surface. The $x/y/z$ direction corresponds to the $a/b/c$ axis in Fig. 1(a). (b) Constant energy mapping at binding energy of −0.2 eV. Incident photon energy is 70 eV. The green dashed lines mark the surface BZ. (c) and (d) ARPES spectrum and corresponding secondary derivative image plot along cut-1 and cut-2 in panel (b). (e) Low energy ARPES spectra crossing the $\bar{\Gamma}$ point for four incident photon energies. (f) Calculated band structures. Black dotted lines are experimental band dispersions extracted from panels (c) and (d). (g) Band dispersion of the highest valence band along Γ–A. Red line is enlarged plot from the greed box in panel (f). Black dots are experimental data extracted from photon energy-dependent measurements. (h) Elements and orbital dependent band structure.

To understand the experimental obtained band structure, we performed first-principles calculations. The calculated bands along high-symmetry directions are presented in Fig. 3(f). Black dots in Fig. 3(f) represent the experimental band dispersions along $\bar{\Gamma}$–$\bar{C}$ and $\bar{\Gamma}$–$\bar{Y}$ direction extracted from Figs. 3(c) and 3(d). The agreement between the experiments and calculations is reasonable. The bulk energy gap obtained in calculation is about 0.2 eV which is slightly smaller than the experimental results. Interestingly, the calculations indicate that the highest valence band and the lowest conduction band are highly anisotropic in its dimensionality. Seen from Fig. 3(f), the calculated bandwidth of the highest valence band along the k_z direction (Γ–A) is very small, while the bandwidth of the lowest conduction band along the k_z direction is much larger (about 1 eV). Enlarged in Fig. 3(g), the calculated bandwidth of the highest valence band along Γ–A direction is only about 0.02 eV. We overlaid the valence band maximum as a function of incident photon energy on the calculated band in Fig. 3(g). Indeed, the observed band dispersion along Γ–A direction is very small. The nearly non-dispersive behavior of

the valence band maximum along the k_z direction means that holes in KAg_3Te_2 could exhibit quasi-two-dimensional behavior, while electrons in the conduction band still exhibit three-dimensional behavior. To understand such extreme anisotropic behavior, we checked the elemental and orbital dependencies of different bands near the Fermi energy, as shown in Fig. 3(h). The size of the dots in Fig. 3(h) indicates the weight of the contribution; the larger the size, the greater the contribution. As seen from Fig. 3(h), $5p_x$ orbital of Te, $4d_{yz}$ and $4d_{z^2}$ orbitals of Ag and all orbitals of K has very little contributions to the highest valence band. The dominant contribution to the highest valence band is $5p_y$ orbital of Te. Because the p_y orbital lies in the plane, the highest valence band is quasi-two-dimensional. For the lowest conduction band, the dominant contribution is from Te $5p_z$ orbital and K 4s orbital, indicating electrons can move in all directions. Therefore, the lowest conduction band is three-dimensional.

Table 1. Experimental data on physical properties of several typical semiconductors near room temperature.

Compound	Band gap (eV)	Effective hole mass (m_e)
KAg_3Te_2[a)]	0.4 ± 0.1	0.12
SnSe	0.86[b)]	0.33[c)]
PbSe	0.27[d)]	0.27[e)]
Black phosphorus[f)]	0.32	0.06

[a)]This work, [b)]Ref. [17], [c)]Ref. [18], [d)]Ref. [19], [e)]Ref. [20], [f)]Ref. [21], at 125 K.

4. Conclusion

In summary, we have investigated the electronic structure of the topological insulator candidate, KAg_3Te_2 single crystals, using electric transport, optical absorption, ARPES, and first-principles calculations. Our experimental results indicate that KAg_3Te_2 exhibits insulating behavior, but is topological trivial. Our samples are of p-type with carrier density of about 6.1×10^{14} cm^{-3}. The energy gap determined from resistivity measurements is about 0.4 eV, and about 0.3 eV from optical absorption measurements. The effective hole mass of KAg_3Te_2 is very small (about 0.12 m_e). We also revealed that the highest valence band is highly quasi-two-dimensional, while the lowest conduction band is three-dimensional. Given its very light hole and pronounced dimensional anisotropy in the electronic structure, KAg_3Te_2 may have potential applications in the future.

Acknowledgements

Project supported by the National Key Research and Development Program of China and the National Natural Science Foundation of China.

References

[1] Witting I T, Chasapis T C, Ricci F, Peters M, Heinz N A, Hautier G and Snyder G J 2019 *Adv. Electron. Mater.* **5** 1800904
[2] Hor Y S, Richardella A, Roushan P, Xia Y, Checkelsky J G, Yazdani A, Hasan M Z, Ong N P and Cava R J 2009 *Phys. Rev. B* **79** 195208
[3] Chen Y L, Analytis J G, Chu J H, Liu Z K, Mo S K, Qi X L, Zhang H J, Lu D H, Dai X, Fang Z, Zhang S C, Fisher I R, Hussain Z and Shen Z X 2009 *Science* **325** 178
[4] Xia Y, Qian D, Hsieh D, Wray L, Pal A, Lin H, Bansil A, Grauer D, Hor Y S, Cava R J and Hasan M Z 2009 *Nat. Phys.* **5** 398
[5] Zhang H, Liu C X, Qi X L, Dai X, Fang Z and Zhang S C 2009 *Nat. Phys.* **5** 438
[6] Burschka C and Bronger W 1977 *Z. Anorg. Allg. Chem.* **430** 61
[7] Rettie A J E, Malliakas C D, Botana A S, Hodges J M, Han F, Huang R, Chung D Y and Kanatzidis M G 2018 *J. Am. Chem. Soc.* **140** 9193
[8] Rettie A J E, Ding J, Zhou X, Johnson M J, Malliakas C D, Osti N C, Chung D Y, Osborn R, Delaire O, Rosenkranz S and Kanatzidis M G 2021 *Nat. Mater.* **20** 1683
[9] Wang C, Cheng R and Chen Y 2023 *Chem. Mater.* **35** 1780
[10] He J, Xia Y, Lin W, Pal K, Zhu Y, Kanatzidis M G and Wolverton C 2022 *Adv. Funct. Mater.* **32** 2108532
[11] Zhang T, Jiang Y, Song Z, Huang H, He Y, Fang Z, Weng H and Fang C 2019 *Nature* **566** 475
[12] Vergniory M G, Elcoro L, Felser C, Regnault N, Bernevig B A and Wang Z 2019 *Nature* **566** 480
[13] Kresse G and Hafner J 1993 *Phys. Rev. B* **48** 13115
[14] Kresse G and Furthmüller J 1996 *Phys. Rev. B* **54** 11169
[15] Perdew J P, Burke K and Ernzerhof M 1996 *Phys. Rev. Lett.* **77** 3865
[16] Monkhorst H J and Pack J D 1976 *Phys. Rev. B* **13** 5188
[17] Zhao L D, Lo S H, Zhang Y, Sun H, Tan G, Uher C, Wolverton C, Dravid V P and Kanatzidis M G 2014 *Nature* **508** 373
[18] Lu Q, Wu M, Wu D, Chang C, Guo Y P, Zhou C S, Li W, Ma X M, Wang G, Zhao L D, Huang L, Liu C and He J 2017 *Phys. Rev. Lett.* **119** 116401
[19] Strauss A J 1967 *Phys. Rev.* **157** 608
[20] Chasapis T C, Lee Y, Hatzikraniotis E, Paraskevopoulos K M, Chi H, Uher C and Kanatzidis M G 2015 *Phys. Rev. B* **91** 085207
[21] Chen Z, Dong J, Giorgetti C, Papalazarou E, Marsi M, Zhang Z, Tian B, Ma Q, Cheng Y, Rueff J P, Taleb-Ibrahimi A and Perfetti L 2020 *2D Mater.* **7** 035027